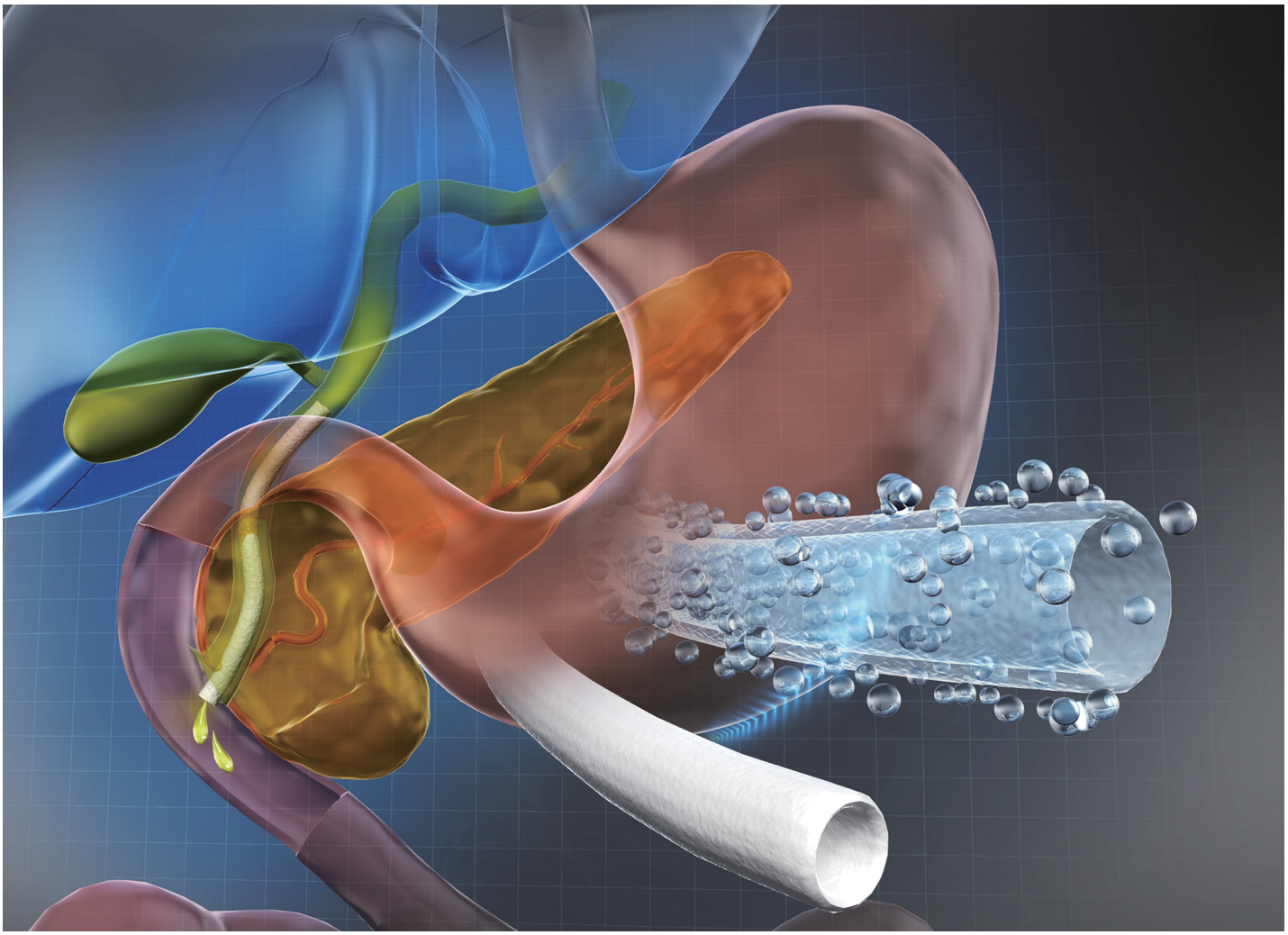

Showcasing research from Dr Yoshiyasu Nagakawa's research group at Tokyo Metropolitan Industrial Technology Research Institute (TIRI), Tokyo, Japan.

Characterization and preliminary *in vivo* evaluation of a self-expandable hydrogel stent with anisotropic swelling behavior and endoscopic deliverability for use in biliary drainage

Poly(vinyl alcohol) (PVA) hydrogel with anisotropic swelling behavior and endoscopic deliverability was used as a self-expandable biliary stent. An *in vivo* experiment using a porcine stent model demonstrated that the PVA hydrogel can expand the biliary tract, without disturbing bile flow.

As featured in:

See Yoshiyasu Nagakawa, Satoshi Fujita *et al.*, *J. Mater. Chem. B*, 2022, **10**, 4375.

ROYAL SOCIETY OF CHEMISTRY

rsc.li/materials-b

Registered charity number: 207890

Journal of Materials Chemistry B

ROYAL SOCIETY OF CHEMISTRY

PAPER

View Article Online
View Journal | View Issue

Cite this: J. Mater. Chem. B, 2022, 10, 4375

Characterization and preliminary *in vivo* evaluation of a self-expandable hydrogel stent with anisotropic swelling behavior and endoscopic deliverability for use in biliary drainage

Yoshiyasu Nagakawa, *[ab] Satoshi Fujita, *[bc] Shunji Yunoki,[a] Takayoshi Tsuchiya,[d] Shin-ichiro Suye,[bc] Kenji Kinoshita,[e] Motoki Sasaki[f] and Takao Itoi[d]

Received 14th January 2022,
Accepted 4th March 2022

DOI: 10.1039/d2tb00104g

rsc.li/materials-b

We demonstrate the potential of a novel self-expandable biliary stent comprised of poly(vinyl alcohol) (PVA) hydrogel with anisotropic swelling behavior and endoscopic deliverability *in vivo*, using a porcine stent model. The mechanism underlying the anisotropic swelling behavior and endoscopic deliverability (*i.e.*, flexibility) was investigated by scanning electron microscopy (SEM), small-angle X-ray scattering (SAXS), evaluation of the water content and swelling ratio, and three-point bending tests. The *in vivo* experiment using a porcine stent model indicated that the tube-shaped PVA hydrogel could effectively expand the biliary tract, without disturbing bile flow. SEM and SAXS showed that PVA hydrogels prepared by drying under extension showed structural orientation along the extension axis, leading to anisotropic swelling. The water content of the PVA hydrogel was found to be crucial for maintaining flexibility as well as endoscopic deliverability. In conclusion, this study demonstrated the novel concept of using a hydrogel stent as a self-expandable biliary stent.

Introduction

Malignant biliary obstruction (MBO) is caused by cholangiocarcinoma, ampullary cancer, and pancreatic cancer.[1–3] MBO is the most prevalent cause of obstructive jaundice, which presents as jaundiced skin, pruritus, nausea, dark urine, and stool discoloration, leading to poor quality of life.[4] Endoscopic biliary stenting is a widely accepted standard palliative therapy for MBO.[5–7] Endoscopic biliary stenting is minimally invasive compared to surgery and percutaneous or nasobiliary drainage, and improves the quality of life and activities of daily living of MBO patients.[8,9] Plastic stents (PSs) and self-expandable metallic stents (SEMSs) with different mechanical characteristics are used for biliary drainage, depending on the MBO symptoms.[10–12]

PSs, first reported in 1980 by Soehendra and Reynders-Frederix,[8] are simple plastic tubes composed of a synthetic polymer, such as polytetrafluoroethylene, polyethylene, or polyurethane.[12] A PS can be easily removed and repositioned and is inexpensive compared to a SEMS.[13] However, the diameter of a PS (up to 3.3 mm) is significantly smaller than that of a SEMS, leading to clogging faster due to biliary sludge adsorption onto the inner surface and subsequent biofilm formation.[14,15] A SEMS, which is a tubular mesh composed of shape-memory alloy, is retracted in a narrow outer sheath of the endoscopic delivery system.[16,17] After delivery into the bile duct *via* an endoscopic working channel, the retracted SEMS is released by withdrawing the outer sheath. Then, it immediately self-expands in the duct to a larger diameter of 6–10 mm, enabling higher bile-flow rates with a later onset of clogging, resulting in a longer patency than that of PSs.[18–20] However, SEMSs are more expensive and more difficult

[a] *Biotechnology Group, Tokyo Metropolitan Industrial Technology Research Institute, 2-4-10, Aomi, Koto-ku, Tokyo, 135-0064, Japan. E-mail: nagakawa.yoshiyasu@iri-tokyo.jp; Fax: +81-3-5530-2629; Tel: +81-3-5530-2671*

[b] *Department of Frontier Fiber Technology and Sciences, Graduate School of Engineering University of Fukui, 3-9-1, Bunkyo, Fukui, 910-8507, Japan. E-mail: fujitas@u-fukui.ac.jp; Fax: +81-776-27-8747; Tel: +81-776-27-9969*

[c] *Life Science Innovation Center, University of Fukui, 3-9-1, Bunkyo, Fukui, 910-8507, Japan*

[d] *Department of Gastroenterology and Hepatology, Tokyo Medical University, 6-7-1, Nishishinjuku, Shinjuku-ku, Tokyo, Japan*

[e] *Industrial Analysis and Inspection Technology Group, Tokyo Metropolitan Industrial Technology Research Institute, 2-4-10, Aomi, Koto-ku, Tokyo, 135-0064, Japan*

[f] *Division of Research and Development for Minimally Invasive Treatment, Cancer Center Keio University School of Medicine, 35, Shinanomachi, Shinjuku-ku, Tokyo, 160-8582, Japan*

to reposition after deployment.[13] One of the most serious problems with SEMSs is tumor ingrowth throughout the metal mesh voids, leading to stent obstruction, rendering removal difficult, and necessitating endoscopic reintervention.[21–23] SEMSs covered with silicone or a polytetrafluoroethylene membrane on the mesh are used to prevent tumor ingrowth; however, problems of migration, tumor overgrowth, and complications with pancreatitis or cholecystitis still remain. Thus, the benefit of covered SEMSs over uncovered SEMSs remains unclear.[23,24] Therefore, the development of a self-expandable stent with a larger inner diameter and good removability is urgently required.

We previously designed a novel self-expandable stent composed of poly(vinyl alcohol) (PVA) hydrogel, exploiting the swelling property of PVA hydrogel as a self-expanding property.[25] PVA is being investigated as a self-expandable material because it has excellent mechanical properties and long-term dimensional stability and can be easily prepared through simple physical crosslinking.[26–28] Furthermore, PVA is eligible for use as an implant material and has already been used in numerous biomedical applications,[29,30] including wound dressings,[31,32] contact lenses,[33] and implants for various tissues and organs, such as cartilage,[34] vascular access,[35] ligaments,[36] and bone tissue engineering applications.[37] Dried tube-shaped PVA hydrogels, which look like conventional PSs, self-expand by swelling in physiological saline, and the radial force of swollen tube-shaped hydrogels is significantly higher than those of conventional SEMSs, indicating that PVA-hydrogel stents are potentially applicable as self-expandable biliary stents.[25] In our previous study, we found that tube-shaped PVA dried under extension shows anisotropic swelling behavior, enabling an approximately two-fold expansion of the inner diameter. However, the mechanism underlying the anisotropic swelling property of PVA hydrogel was not identified. Furthermore, although our previous study revealed that the radial force of tube-shaped PVA hydrogel was higher than that of conventional SEMSs, it remained unclear whether it can expand in tissues *in vivo*.

In this study, we investigated the anisotropic swelling behavior of tube-shaped PVA hydrogel by changing the extension ratio. The dimensional ratio of the inner diameter of the tube-shaped PVA hydrogel increased as the extension ratio increased, whereas its length decreased. Scanning electron microscopy (SEM) and X-ray diffraction analyses demonstrated that dried PVA hydrogel forms oriented structures that lead to anisotropic swelling. Endoscopic deliverability was achievable by controlling the water content of the dried PVA. In an *in vivo* experiment using a porcine stent model, we observed expansion of the bile duct, indicating that the tube-shaped hydrogel is applicable as a self-expandable biliary stent.

Experimental

Materials

PVA powder (grade, PVA-117, saponification degree, 98.0–99.0, polymerization degree, 1700) was kindly provided by Kuraray Co., Ltd. (Tokyo, Japan). Sodium sulfate (Na_2SO_4), sodium chloride (NaCl), barium sulfate ($BaSO_4$), glutaraldehyde (GA; 25% solution), Coomassie Brilliant Blue (CBB) solution (Quick-CBB Plus), toluidine blue (TB) solution (0.05% solution, pH 7.0) (all from Fujifilm Wako Pure Chemical Industries, Osaka, Japan), paraformaldehyde (4% solution; Nacalai Tesque, Kyoto, Japan), and carboxymethyl cellulose (CMC) (4% CMC sodium salt; Leica Microsystems, Wetzlar, Germany) were purchased and used without further purification.

PVA hydrogel fabrication

PVA hydrogels with tube and rectangular shapes were fabricated as described in our previous report.[25] Briefly, PVA powder was dissolved in hot water (100 °C) at a concentration of 10 w/w%. Sodium sulfate solution (2 M) was gradually added to the PVA solution under agitation to achieve a final concentration of 0.45 M, resulting in the precipitation of the PVA.[38] The precipitated PVA was transferred into a 50 mL tube and centrifuged at 4500 rpm for 3 min to obtain a dense precipitate without air bubbles and then poured into two types of molds: disc-shaped (biological dish with a 50 mm diameter and 2–3 mm thickness) and custom-made tube-shaped (polytetrafluoroethylene; length: 80 mm, inner diameter (I.D.): 5 mm, and outer diameter (O.D.): 8 mm). The molds were placed in a freezer and subjected to a cycle of freezing (−30 °C for 12 h) and subsequent thawing (25 °C for 1 h) to produce the disc-shaped and tube-shaped PVA hydrogels. Rectangular-shaped PVA hydrogels were cut from the disc-shaped hydrogels.

Tube-shaped hydrogel specimens were dried at 60 °C in an oven to various extension ratios, as described in our previous report.[25] Both ends of the hydrogels were penetrated with silk strings. The hydrogels were placed vertically in a drying chamber (600 mm × 500 mm × 500 mm) at 60 °C under tension: one end of the hydrogel was anchored to the ceiling of the chamber with the silk string and the other end was attached to weights to achieve length extension ratios of 1.5, 2.0, and 2.5. After drying, both ends of the hydrogel (approximate length, 25 mm) were cut from the specimen to remove the penetrated parts. Dried tube-shaped hydrogel specimens without extension were also prepared from tube-shaped PVA hydrogels by not attaching weights, and their extension ratio was set to 1.0.

Characterization of the tube-shaped PVA hydrogels

Analysis of the dimensional changes induced by swelling. Dimensional changes of the dried tube-shaped PVA hydrogels with extension ratios of 1.0, 1.5, 2.0, and 2.5 upon swelling in physiological saline were investigated using a slightly modified version of our previously reported method, as shown in Scheme 1.[25] The dimensions (I.D.(ID_d), O.D.(OD_d), and length (L_d)) of the dried tube-shaped hydrogels were measured using a caliper and then, the hydrogels were immersed in physiological saline (0.9% NaCl) at 37 °C. After immersion for 72 h, the dimensions (I.D.(ID_s), O.D.(OD_s), and length (L_s)) of the reswollen, saturated hydrogels were measured again. The dimensional changes were expressed as the ratio of the dimensions before and after swelling (ID_s/ID_d, OD_s/OD_d, and L_s/L_d). The dimensional

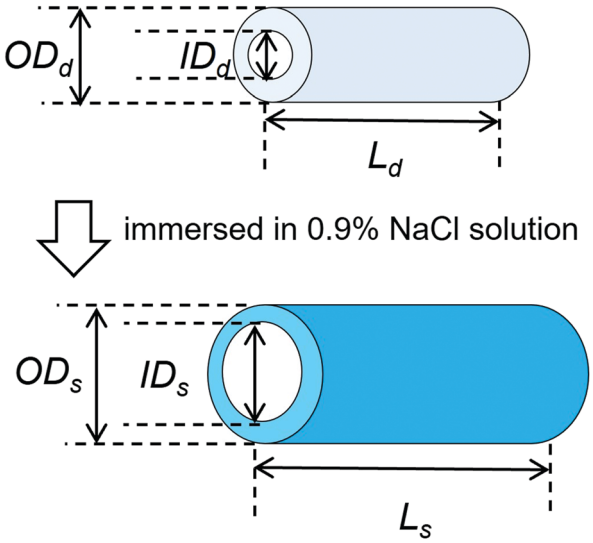

Scheme 1 Illustration of the dimensional changes test. The dimensional changes of the inner diameter (I.D.), outer diameter (O.D.), and length were expressed as ID_s/ID_d, OD_s/OD_d, and L_s/L_d, respectively.

changes of dried tube-shaped PVA hydrogels with an extension ratio of 2.0 were determined at certain time points (0, 1, 3, 6, 12, 24, 48, and 72 h).

Surface morphology observation

The morphologies of the dried tube-shaped PVA hydrogels were observed by SEM using a TM4000Plus microscope (Hitachi High-Technologies, Tokyo, Japan) at an acceleration voltage of 15 kV. The center of the dried specimens with extension ratios of 1.0–2.5 was cut with scissors. The specimens were dried using *t*-butyl alcohol and coated with Au.

Structural analysis

The structures of the dried tube-shaped PVA hydrogels were determined through small-angle X-ray scattering (SAXS) measurements using a SAXSpoint5.0 instrument (Anton Paar, Graz, Austria) with a wavelength λ of 0.1542 nm, at 1 kV and 50 mA. The two-dimensional (2D) scattering intensity of the samples at 30 min was measured using an X-ray Eiger2 R 1M detector (Dectris, Zürich, Switzerland). The dried specimens with extension ratios of 1.0–2.5 were set parallel and perpendicular to the meridional axis of the X-ray detector to analyze the structures parallel and perpendicular to the extended axes. The scattering vector, $q = (4\pi/\lambda)\sin\theta$, where θ is the scattering angle, was calibrated using silver behenate. One-dimensional (1D) profiles were calculated by sector-averaging the 2D SAXS patterns within a sector angle of 45° with the meridional axis. Long-period structures were evaluated according to Bragg's law, $2\pi/q$, where q is the peak position value (q_{max}), plotted against $q^2I(q)$ as a function of q.[39]

Water content evaluation

The water contents (WCs) of the PVA hydrogels were controlled by changing the drying time. The weights of the rectangular PVA hydrogels dried at 60 °C for 0, 3, 6, 12, 24, 48, and 96 h (W_d) were measured. The weights of the completely dried samples after drying in a vacuum oven at 120 °C for 48 h (W_{dc}) were measured as well. The WCs of the specimens were calculated as $(W_d - W_{dc})/W_d \times 100$.

Swelling tests

The swelling ratios (SRs) of the PVA hydrogels were evaluated by swelling in physiological saline. The PVA hydrogels were dried at 60 °C for 0, 3, 6, 12, 24, 48, and 96 h and their weight (W_d) was measured. Subsequently, they were immersed in physiological saline at 37 °C for 72 h and their weight (W_s) was measured. The SRs of the specimens were expressed as W_s/W_d.

Three-point bending tests

The flexural moduli of the rectangular specimens were evaluated using a texture analyzer (TA.XTplus; Stable Micro Systems, Godalming, UK), with a slightly modified version of a previously described method.[40] Rectangular specimens with various WCs were bent in a span of 30 mm at a crosshead speed of 1 mm s^{-1}. The flexural modulus (MPa) was calculated from the stress and strain data at a strain of 0.5 mm using the following equation:

$$\text{Flexural modulus} = L^3F/4bh^3Y,$$

where L is the span (mm), F is the stress, b is the width of the specimen (mm), h is the height of the specimen (mm), and Y is the strain. The tests were quickly conducted at room temperature, which highly reduced the potential effect of water loss from the specimens on the flexural moduli.

The flexural load of the tube-shaped PVA hydrogel with an extension ratio of 2.0 and a 6 h drying time was compared with commercially available PS using the texture analyzer. The samples were bent in a span of 30 mm at a crosshead speed of 1 mm s^{-1}. The PS (Flexima™, Boston Scientific, Marlborough, MA, USA) was used as a control. The I.D., O.D., and length of tube-shaped PVA hydrogels and PS were 2.5 mm and 2.0 mm, 3.5 mm and 2.8 mm, and 40 mm for both, respectively.

In vivo experiment

Preparation of tube-shaped PVA hydrogel for use in the *in vivo* experiment. The tube-shaped PVA hydrogel for use in the *in vivo* experiment was prepared as described above, except that $BaSO_4$ was added to enable radiographic visualization, which allows for endoscopic stenting. $BaSO_4$ was added into the PVA solution before Na_2SO_4 addition. The extension ratio and drying time of the dried tube-shaped PVA hydrogel used *in vivo* were 2.0 and 6 h, respectively, and the I.D., O.D., and length were 2.5 mm, 3.5 mm, and 40 mm, respectively.

In vivo experiment using a porcine stent model

The Animal Ethics Committee of the Laboratory Animal Center of Keio University School of Medicine, Tokyo, Japan approved the animal experiment using a porcine stent model. The animal experiment was carried out in the laboratory animal center of Keio University School of Medicine. A pig was fasted the night before the procedure. The animal was medicated intramuscularly

with midazolam (2 mg kg^{-1}), medetomidine hydrochloride (80 μg kg^{-1}), and atropine (20 μg kg^{-1}). Ravonal (1 mg kg^{-1}) was administered intravenously in accordance with anesthetic depth. After tracheal intubation, isoflurane (2%) was further administered to maintain anesthesia. The animal was placed in the supine position on the fluoroscopy table of an ARCADIS Avantic instrument (Siemens Healthineers, Erlangen, Germany). Vital signs were monitored continuously during the experiment. The animal was subjected to endoscopic biliary stenting with the dried tube-shaped PVA hydrogel using a standard duodenoscope (ED-580T; Fujifilm, Tokyo, Japan). During the deployment procedure, bile duct appearance was delineated under fluoroscopy and endoscopic visualization. The animal was fed a standard diet for four weeks following the successful stent placement. The tube-shaped PVA hydrogel was removed using forceps under endoscopic control with the same delineation as for deployment. Bile was collected from the pig after euthanasia with a potassium chloride overdose.

Evaluation of the tube-shaped PVA hydrogel *in vivo*

Analysis of the dimensional changes induced by swelling *in vivo*. The dimensional changes of the tube-shaped PVA hydrogel implanted in the porcine bile duct were investigated as described above. The dimensions (I.D., O.D., and length) of the dried tube-shaped hydrogel were measured using a caliper before deployment and after removal from the porcine bile duct, and the dimensional ratios were determined. The dimensional ratios of a tube-shaped PVA hydrogel swollen in physiological saline were used as a control.

Characterization of adherent substance on the tube-shaped hydrogel *in vivo*

Microscopic observation. The appearance of the hydrogel explanted from the porcine bile duct was observed using a digital microscope (VHX-7000; Keyence, Osaka, Japan). After removal and dimensional ratio evaluation, the hydrogel was gently immersed in phosphate-buffered saline (PBS) for 10 min to remove the bile. The explanted hydrogel was cut longitudinally to observe the lumen surface. The control hydrogel swollen in physiological saline was treated in the same manner and observed for comparison.

After the microscopic observation, the tube-shaped PVA hydrogel was fixed in 4% paraformaldehyde and 2.5% glutaraldehyde in PBS at 4 °C for 30 min. The sample was washed with PBS for 10 min three times and embedded in CMC. After freezing by immersion in isopentane at −80 °C, the sample block was cut into 10 μm-thick sections using a microtome (CM3050S; Leica Microsystems, Wetzlar, Germany), which were collected on microscope slide glasses. The samples were stained with CBB or TB solution. The appearance of the samples was observed under a light microscope (BX53; Olympus, Tokyo, Japan).

Fourier-transform infrared spectroscopy. The adherent material on the explanted hydrogel observed through microscopy was investigated using attenuated total reflection Fourier-transform (ATR-FTIR) spectroscopy (FT/IR-6100TypeA; JASCO Corporation, Tokyo, Japan). Part of the adherent material was collected using forceps. Spectra were acquired at 4000–500 cm^{-1} at a resolution of 4 cm^{-1} using a KBr detector, with 64 scans.

Results

Effect of drying under extension on the swelling behavior of tube-shaped hydrogels

The changes in the dimensional ratios as a function of the extension ratios are shown in Fig. 1a. Anisotropic swelling was observed in the drying and extending tube-shaped PVA hydrogels. Isotropic swelling was observed in the non-extended tube-shaped PVA hydrogel, and the dimensional ratios of I.D., O.D., and length were 1.4–1.5. Conversely, the dimensional ratios of the I.D. and O.D. of the tube-shaped PVA hydrogels with an extension ratio of 1.5 were increased to 1.7 ± 0.02 and 2.0 ± 0.05, respectively, whereas the ratio of their length was decreased to 0.86 ± 0.01. Similar trends were observed for the hydrogels with extension ratios of 2.0 and 2.5. The dimensional ratios of I.D., O.D., and length for hydrogels with an extension ratio of 2.0 were 2.0 ± 0.05, 2.1 ± 0.03, and 0.76 ± 0.01, respectively. The dimensional ratios of the I.D. and O.D. for hydrogels with an extension ratio of 2.5 were slightly further increased, at 2.1 ± 0.05 and 2.3 ± 0.04, whereas the ratio of their length was decreased to 0.63 ± 0.01.

The changes in the dimensional ratios of the tube-shaped PVA hydrogel with the extension ratio of 2.0 as a function of time are shown in Fig. 1b. All dimensional ratio values sharply increased at the beginning of the immersion in physiological saline at 37 °C and reached a plateau after 24 h of immersion. The dimensional change rates in I.D. immersed in physiological saline at 1, 3, and 6 h were approximately 64%, 84%, and 97%, respectively, indicating that expansion due to swelling in physiological saline was nearly completed within 6 h.

Effect of drying under extension on the structure of the dried tube-shaped hydrogels

SEM images of the surface morphologies of the dried tube-shaped hydrogels with or without extension are shown in Fig. 2. The surface morphology appeared to be extended along the stretch axis and more obviously so with increasing extension ratio. An isotropic structure was observed in non-extended dried-tube-shaped hydrogel (Fig. 2a). In the extended specimens, the surface morphologies were extended along the stretch axis (Fig. 2b–d).

The structures of the dried tube-shaped hydrogels were further evaluated by SAXS (Fig. 3). Isotropic scattering was observed in the SAXS 2D patterns of the non-extended dried tube-shaped hydrogel (Fig. 3a and e). For the extended specimens, the 2D scattering patterns revealed increasingly anisotropic behavior as the extension ratio increased both parallel (Fig. 3b–d) and perpendicular to the extension direction along the meridional axis of the X-ray 2D detector (Fig. 3f–h). The 1D profiles calculated from the 2D scattering patterns plotted against $q^2I(q)$ as a function of q are shown in Fig. 3i and j. Parallel to the extension direction, q_{max} shifted to a lower value as the extension

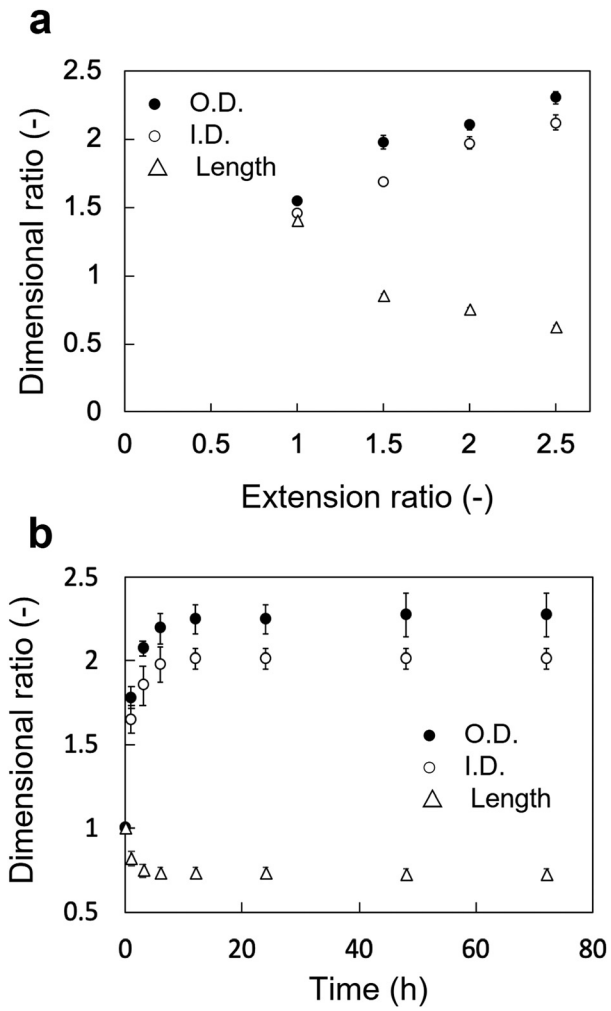

Fig. 1 Changes in the dimensional ratios of the outer diameter (O.D.), inner diameter (I.D.), and length of tube-shaped PVA hydrogels as a function of (a) the extension ratio and (b) the immersion time in physiological saline for a hydrogel with an extension ratio of 2.0. Data are presented as the mean ± SD (n = 3).

ratio increased, but this trend was nearly saturated at an extension ratio of 2.0 (Fig. 3i). Moreover, long periods were calculated from the q_{max} obtained in the 1D profiles using Bragg's law $2\pi/q_{max}$ and plotted as a function of the extension ratio (Fig. 3k). The long period of the dried tube-shaped hydrogel without extension parallel to the extension direction was calculated to be 8.2 ± 0.1 nm. The long period increased to 9.4 ± 0.2 nm at the extension ratio of 1.5, and was nearly saturated at 9.8–10 nm at the extension ratios of 2.0 and 2.5. The change in q_{max} perpendicular to the extension direction was smaller than that in the parallel direction (Fig. 3j); the long period at the extension ratio of 1.0 was calculated to be 8.0 ± 0.03 nm and reached 7.0 ± 0.4 nm at the extension ratio of 2.5 (Fig. 3k). These trends were similar to those reported previously.[39,41]

Effect of WC on the flexibility and swelling property of the PVA hydrogels

The changes in the WC of the rectangular PVA hydrogels as a function of the drying time are shown in Fig. 4a. The WC of rectangular PVA hydrogel sharply decreased at the beginning of drying at 60 °C and reached a plateau after 24 h. The initial WC of the rectangular PVA hydrogel was 70 ± 0.15%. The WCs after 3, 6, 12, 24, 48, and 96 h of drying were 28 ± 4%, 20 ± 1%, 14 ± 2%, 9.6 ± 0.7%, 6.3 ± 0.6%, and 5.7 ± 0.6%, respectively.

The flexural moduli and SRs of the rectangular PVA hydrogels as a function of WC are shown in Fig. 4b. The change in the flexural moduli showed a moderately sloped region (70–20% WC) and a sharply sloped region (20–5.7% WC). The flexural moduli corresponding to 70%, 28%, and 20% WC were 5.7 ± 1 MPa, 49 ± 10 MPa, and 180 ± 30 MPa, respectively. They sharply increased from 390 ± 150 MPa (14% WC) to 2700 ± 210 MPa (5.7% WC), indicating that flexibility rapidly decreased. In contrast, the SRs of the PVA hydrogels increased rather linearly with decreasing WC. The initial SR value (70% WC) was 1.3 ± 0.03, indicating slight swelling. The SR value linearly increased to 2.7 ± 0.05 (20% WC) and was nearly saturated at 3.0 ± 0.02 (14% WC). The force–deformation curves of the tube-shaped hydrogel and commercially available PS obtained from the three-point bending tests are shown in Fig. 4c. The curve of hydrogel was similar to that of PS, indicating that the PVA hydrogel dried for 6 h had a flexibility sufficient for endoscopic deliverability. Therefore, this PVA hydrogel with good flexibility was used in the subsequent *in vivo* experiment.

In vivo evaluation of the potential of tube-shaped hydrogel as a self-expandable biliary stent

***In vivo* evaluation using a porcine stent model.** The tube-shaped PVA hydrogel could be deployed using a conventional endoscope, without getting stuck in the access channel (Fig. 5). The $BaSO_4$ contained in the hydrogel was sufficient for immediate radiographic visualization (Fig. 5a) and four weeks (Fig. 5b and c)

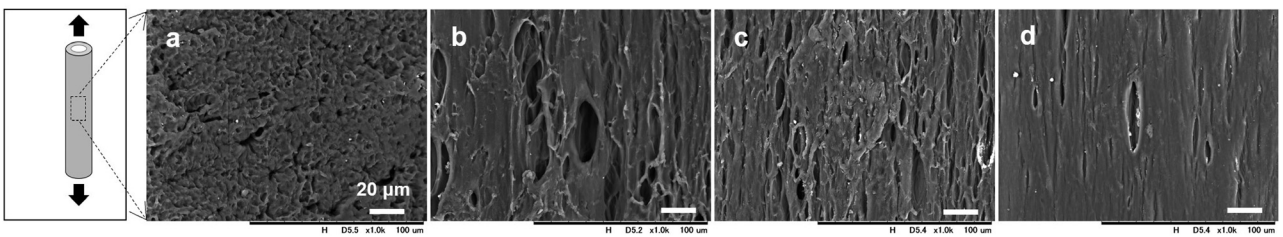

Fig. 2 SEM images showing the surface morphologies of dried tube-shaped hydrogels schematically illustrated in the observed part, with extension ratios of (a) 1.0, (b) 1.5, (c) 2.0, and (d) 2.5. The arrows in the illustration indicate the extension direction of the samples.

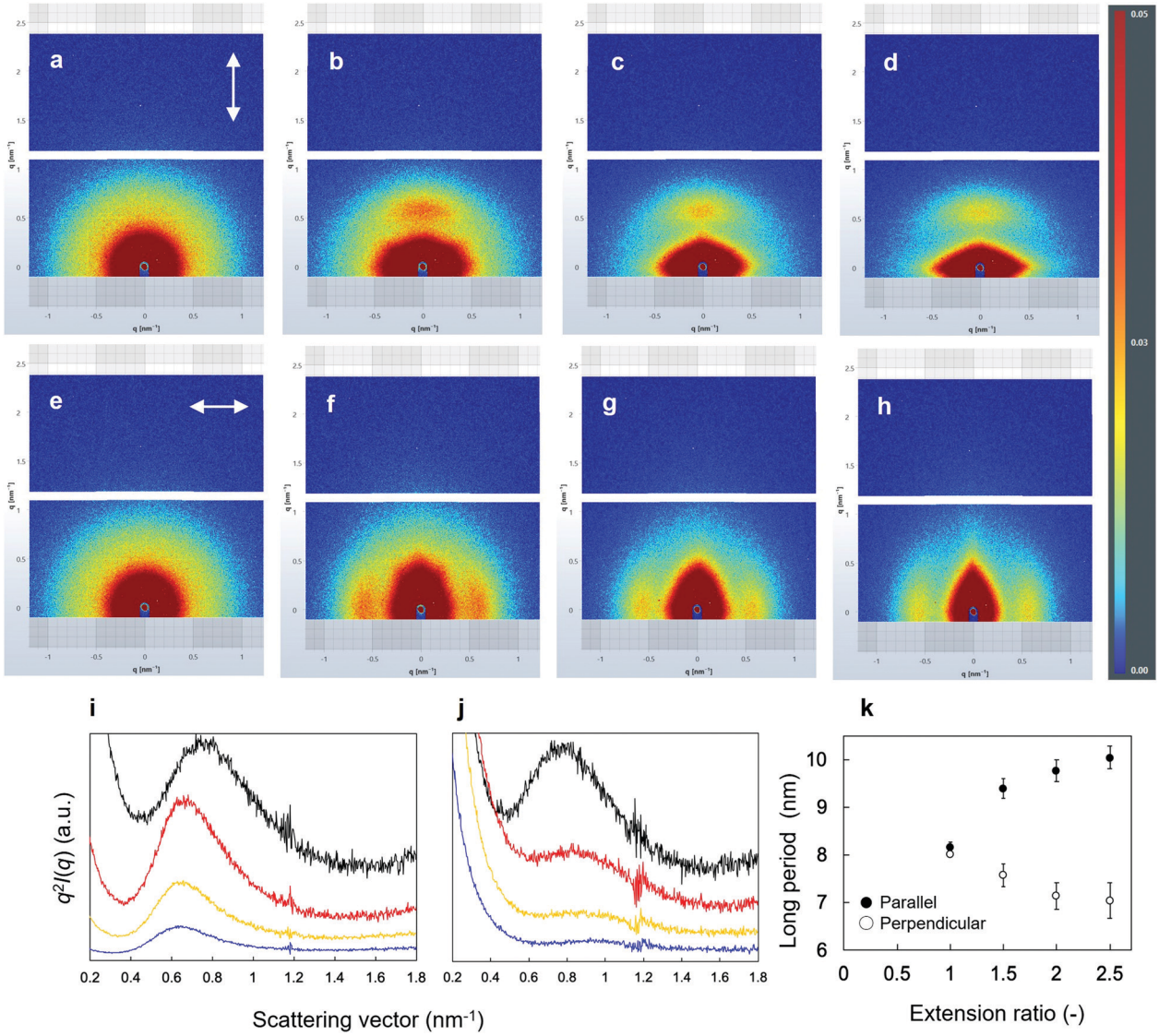

Fig. 3 Small-angle X-ray scattering (SAXS) analysis of dried tube-shaped hydrogels. (a)–(d) 2D scattering patterns of dried tube-shaped hydrogels parallel to the extension direction along the meridional axis of the X-ray detector, with extension ratios of (a) 1.0, (b) 1.5, (c) 2.0, and (d) 2.5. (e)–(h) 2D scattering patterns of dried tube-shaped hydrogels perpendicular to the extension direction along the meridional axis of the X-ray detector, with extension ratios of (e) 1.0, (f) 1.5, (g) 2.0, and (h) 2.5. The arrows in (a) and (e) indicate the extension direction of the samples. (i), (j) 1D profiles of dried tube-shaped hydrogels with extension ratios of 1.0 (black), 1.5 (red), 2.0 (yellow), and 2.5 (blue) at (i) parallel and (j) perpendicular directions to the sector-averaged axis calculated from 2D scattering patterns plotted against $q^2I(q)$ as a function of q. (k) Long periods of the dried tube-shaped hydrogels at parallel and perpendicular directions to the extension axis as a function of the extension ratio. Data in (k) are presented as the mean ± SD (n = 3).

after deployment. Bile flow was confirmed using an endoscopic camera, indicating that implanted hydrogel did not disturb the bile flow. Furthermore, the hydrogel could be removed without breaking, using endoscopic forceps. These results indicate that the tube-shaped hydrogel has potential as a self-expandable biliary stent.

Dimensional changes of tube-shaped PVA hydrogel *in vivo*. Fig. 6 shows the dimensional ratios of the hydrogel explanted from the porcine bile duct in comparison with those of a hydrogel immersed in physiological saline as a control. The I.D., O.D., and length were 4.5 mm, 6.9 mm, and 30 mm, respectively. The dimensional ratios of the I.D. and O.D. of explanted and control hydrogels were both 1.8 and 2.0, indicating that hydrogel expansion *in vivo* was not restricted by the bile duct wall.

Microscopic observation of explanted tube-shaped PVA hydrogel

Images of the tube-shaped hydrogel explanted from the porcine bile duct after four weeks of implantation and hydrogel immersed in physiological saline are shown in Fig. 7. The explanted hydrogel had a yellow color, whereas the control specimen had maintained its original white color. White dots, which were $BaSO_4$ powder, were observed in both the implanted and control hydrogels. Although nearly the entire lumen surface of the explanted hydrogel could be observed (Fig. 7a), some adherent material was observed as well (Fig. 7c).

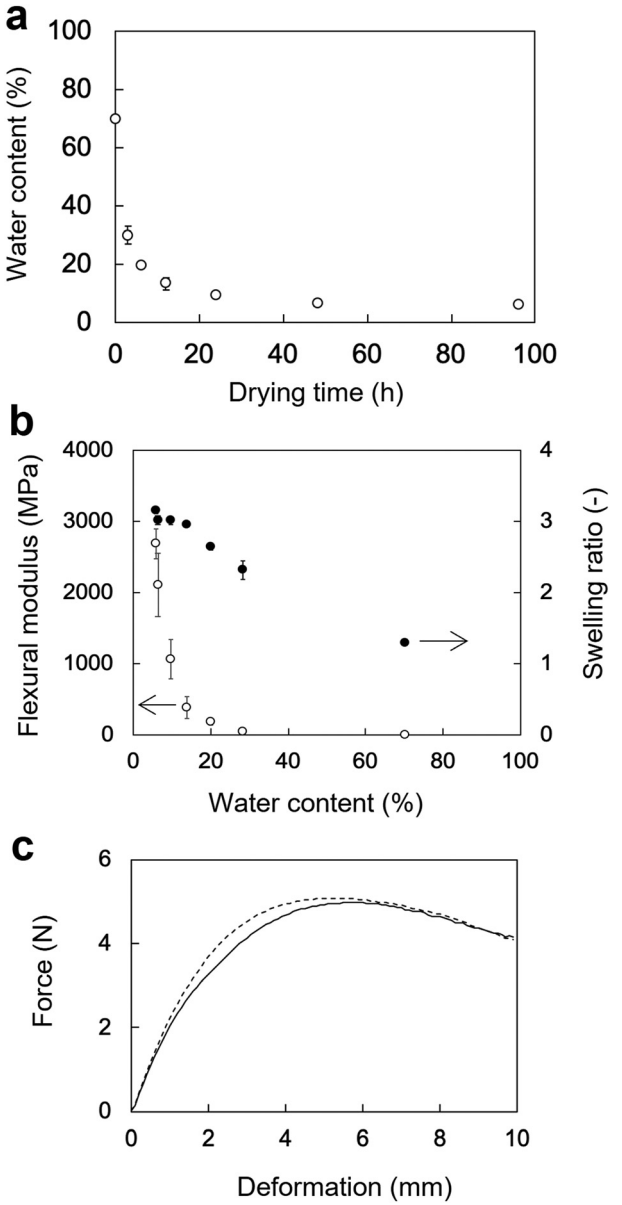

Fig. 4 (a) Water contents (WC) of rectangular PVA hydrogels as a function of drying time. (b) Flexural moduli and swelling ratios of rectangular PVA hydrogels as a function of WC. Data are presented as the mean ± SD (n = 3). (c) Force–deformation curves of the tube-shaped PVA hydrogel (solid line) and PS (dotted line).

Sections of the tube-shaped hydrogel with the adherent material and control hydrogel were stained in CBB and TB solutions. The PVA hydrogel was not stained by CBB nor by TB (Fig. 8). An unstained section and sections stained with CBB and TB are shown in Fig. 8a, b, and c, respectively. The material adhering to the lumen surface of the tube-shaped hydrogel was stained by both CBB and TB, showing a blue and light blue color, respectively.

IR spectrum of the adherent material on the tube-shaped PVA hydrogel *in vivo*

The chemical composition of the adherent material was examined by ATR-FTIR spectroscopy (Fig. 9). Characteristic peaks of

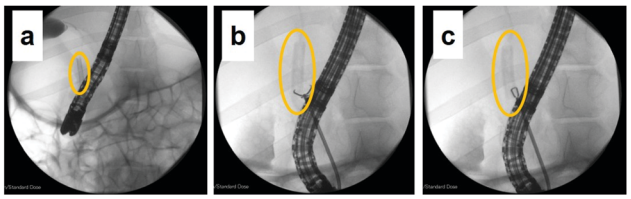

Fig. 5 Fluoroscopy of the porcine stent model *in vivo*. (a) Fluoroscopy immediately after implantation of the tube-shaped hydrogel. The tube-shaped hydrogel is indicated by a circle. (b, c) Fluoroscopy of endoscopic removal after four weeks of implantation. The tube-shaped hydrogel was gripped with forceps and could be removed without breakage. The tube-shaped hydrogel is indicated by a circle.

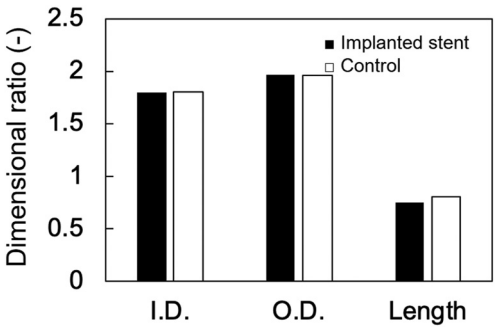

Fig. 6 Dimensional ratios of the I.D., O.D., and length of tube-shaped PVA hydrogels implanted in the porcine bile duct (closed bars) and immersed in physiological saline as a control (open bars).

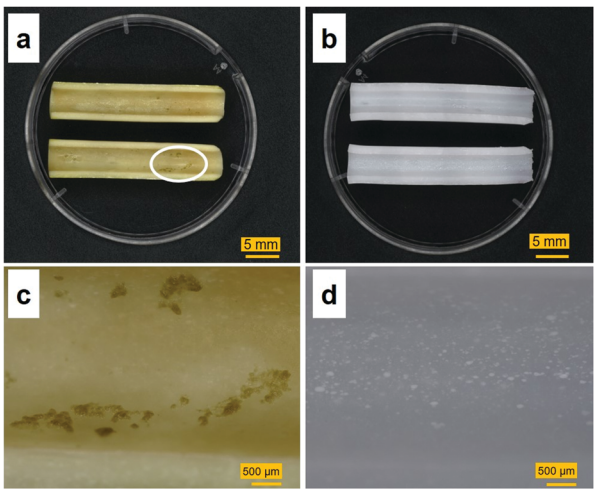

Fig. 7 Appearances of the reswollen tube-shaped hydrogels. Digital microscopic overviews of the reswollen tube-shaped hydrogels (a) implanted in the porcine bile duct and (b) immersed in physiological saline as a control. (c) Magnification of region in (a) indicated in white circle. (d) Magnification of the reswollen tube-shaped hydrogel shown in (b).

adherent material were identified at 1650 cm^{-1} (amide I) and 1540 cm^{-1} (amide II), which are typical of protein. The IR spectrum of the adherent material was compared with that of bile collected from the euthanized porcine stent model (Fig. 9).

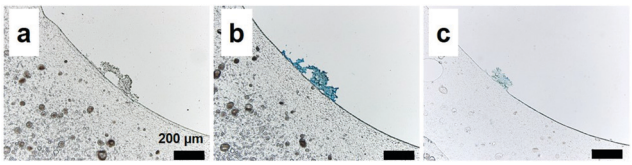

Fig. 8 Microscopic images of sections obtained from the reswollen tube-shaped hydrogel with adherent material after four weeks of implantation in the porcine bile duct. (a) Unstained, (b) stained with Coomassie brilliant blue, and (c) stained with toluidine blue.

A peak at 2920 cm^{-1} was observed in the spectrum of the porcine bile, whereas the amide I and II bands were not observed.

Discussion

This is the first study to evaluate the potential of PVA hydrogel as a self-expandable biliary stent *in vivo*. It is well accepted that one limitation of hydrogels for biomedical application is their poor mechanical properties compared to traditional engineering materials such as alloys and plastics.[42] Furthermore, the swelling of hydrogels is also an unfavorable property because it lowers polymer density as well as mechanical properties.[43] However, we attempted to exploit the swelling property as a self-expanding property for use in self-expandable biliary stents. To investigate the usability of hydrogels in biliary stents, we used PVA hydrogel because it maintains favorable characteristics when used in implantable medical devices: it is physically cross-linkable by a simple freezing/thawing method, the hardness and stiffness of the hydrogel can be modulated while maintaining its swelling property, it is biologically safe, and it is a low-cost polymer. We previously demonstrated that PVA hydrogel-based stents are potentially applicable as self-expandable biliary stents because the radial force of tube-shaped PVA hydrogel was higher than that of commercially available SEMSs.[25] In this study, we demonstrated the potential of anisotropically swelling tube-shape PVA hydrogels as a self-expandable biliary stent in a porcine stent model.

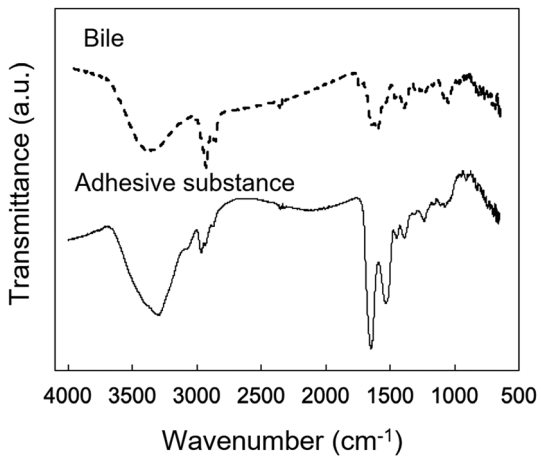

Fig. 9 Microscopic IR spectra of bile obtained from the pig and the adherent material obtained from the reswollen tube-shaped hydrogel explanted from the porcine bile duct.

Like conventional biliary stents, dried tube-shaped PVA hydrogel can be delivered and deployed through an endoscope working channel (Fig. 5). Flexible properties (*i.e.*, low flexural modulus) are essential for devices used with endoscopy because the working channel in the gastrointestinal tract is inevitably tortuous. The drying time of the tube-shaped hydrogel used in the *in vivo* experiment was 6 h. We selected this drying time based on the results of the three-point bending tests (Fig. 4b). The force–deformation curve of tube-shaped PVA hydrogel was similar to that of commercially available PS, which indicated that PVA hydrogel had sufficient flexibility for endoscopic delivery (Fig. 4c). After deployment, the tube-shaped hydrogel expanded by swelling in the bile fluid, without a decrease in the dimensional ratios after four weeks (Fig. 6). Moreover, the hydrogel could be easily removed without breaking using endoscopic forceps and did not adhere to the surrounding biliary tract. These results clearly indicate that tube-shaped PVA hydrogel can be applied as a self-expandable biliary stent. Furthermore, nearly the entire lumen surface of the explanted hydrogel could be observed, with a limited amount of adherent material, after four weeks of deployment. The hydrophilic surface of the PVA hydrogel may have averted protein adhesion onto the lumen surface; it is known that the hydrophilic surface of hydrogel shows low protein adsorption.[44] Microscopic observation of sections stained with CBB and ATR-IR measurement suggested that the adherent material was mainly composed of protein (Fig. 8 and 9). Another potential reason for the low material adsorption is the large I.D. of the swollen tube-shaped PVA hydrogel. Deprez *et al.* reported that the median patency days of 12-Fr (4 mm) PS are more than two times longer than those of 10-Fr (3.3 mm) PS,[45] indicating that I.D. size is critical to patency duration. The I.D. of the reswollen tube-shaped PVA hydrogel was approximately 5 mm. Therefore, tube-shaped hydrogel is expected to show longer patency than conventional PSs.

The anisotropic swelling behavior of the tube-shaped hydrogel is a crucial factor for deployment; the dried tube-shaped PVA hydrogel takes an I.D. of 5 mm after swelling, whereas the endoscopic working channel is limited to 4.2 mm. The dimensional ratios of the I.D. and O.D. of the non-extended tube-shaped hydrogel were both 1.4–1.5, which indicates isotropic swelling. Conversely, drying and consequent extension of the tube-shaped hydrogel increased the dimensional ratios of both I.D. and O.D. to approximately 2, resulting in a large I.D. (approximately 5 mm). The anisotropic swelling property can be obtained simply by drying under extension. The anisotropic swelling property became more obvious as the extension ratio increased (Fig. 1a): the dimensional ratios of the I.D. and O.D. increased with increasing extension ratio, whereas that of the length decreased. Shortening of the tube-shaped hydrogel was significant at the extension ratio of 2.5. As clinicians in gastrointestinal medicine regard self-expandable stents that exhibit substantial shortening unsuitable, an appropriate extension ratio when fabricating tube-shaped hydrogels for use in biliary stents is needed. Additionally, the I.D. dimensional ratio change rates of tube-shaped hydrogels immersed in physiological saline after 1, 3, and 6 h were 64%,

84%, and 97%, respectively, in line with our previous findings.[25] These results suggest that the dried tube-shaped hydrogel expands immediately in the bile after being deployed in the bile duct.

We investigated the morphology and structure of dried tube-shaped PVA hydrogel to clarify the anisotropic swelling property. As shown in Fig. 2, the surfaces of dried specimens were extended along the stretch axis, and more strongly so as the extension ratio increased. Although SEM can reveal the morphology (*i.e.*, local structure) of a sample, it is difficult to analyze the average structure. Thus, we also conducted SAXS analysis to investigate the inner structure of the PVA hydrogel. It is known that a long period structure is related to the total thickness of the lamellar and amorphous layer, and can be observed in a lower q region compared to the crystalline peak.[27,46] Anisotropy clearly increased with an increasing extension ratio in the direction parallel to the extension axis; q_{max} shifted to a lower value, resulting in an increased long period (Fig. 3i and k). However, the shift to a lower q was not significant, even when the extension ratio was increased from 2.0 to 2.5. It was reasonable that the change in the long period perpendicular to the extension axis was smaller than that in the parallel direction (Fig. 3j and k) as the strain of the long period structure in the perpendicular direction should be limited compared to that in the parallel direction. Similar results have been previously reported.[39] In our experiment, the long period structure of PVA may be nearly completely stretched when the extension ratio reaches 2.0. Based on the SEM and SAXS results, we speculate the mechanism of anisotropic swelling to be as follows. During drying under extension, the long period structures of PVA orient to a stretched direction and preserve the structure. Anisotropic swelling occurs during immersion in a solvent, reversing the isotropic structure to some extent.

Our previous study investigated the swelling and mechanical properties of PVA hydrogel in the equilibrium state.[25] Drying time is a crucial factor determining the flexibility an endoscopic deliverability of a PVA hydrogel. The WC of the PVA hydrogel steeply decreased immediately after the start of drying (Fig. 4a). The SR of the PVA hydrogel linearly increased with decreasing WC and was nearly saturated at a WC of 14%. In contrast, the flexural modulus moderately increased when the WC decreased from 70% to 14%, and sharply increased at a WC of 5.7% (Fig. 4b). These results suggest that the water in the PVA hydrogel behaves as a plasticizer, disturbing crystal formation between PVA chains. Crystal formation in PVA hydrogels appears limited when the WC ranges from 70% to 14%. When the WC is below 14%, crystallization likely proceeds rapidly, resulting in a sharp decline in flexibility. In fact, the rectangular specimens with WCs of 6.3 $\pm$ 0.6% and 5.7 $\pm$ 0.6% broke in three-point bending tests. Thus, the WC of a PVA hydrogel is important for maintaining endoscopic deliverability. Alternatively, plasticizer could be added to the PVA hydrogel to maintain flexibility and endoscopic deliverability.

Although tube-shaped PVA hydrogel with optimized extension ratio and WC could effectively expand the porcine bile duct, some adherent material was observed (Fig. 7a and c). It is well accepted that the major causes of biliary stent occlusion are biliary sludge and bacterial biofilm formation. The adherent material was characterized through microscopic observation of sections stained with CBB and TB to clarify its composition (Fig. 8). The adherent material stained blue with CBB, indicating that it was composed of protein, which was confirmed by the IR spectra (Fig. 9). The adherent material stained light blue with TB (Fig. 8c), indicating only background staining.[47] Biofilms are composed of polysaccharide, proteins, humic substances, and lipids.[48,49] If the adherent material would have included biofilm compounds, it would have stained purple with TB. Thus, we consider that biofilm formation did not occur *in vivo* in the current experiment. The four-week implantation period may have been too short for biofilm formation to occur. Lee *et al.* reported that SEMSs covered with silver particle-integrated silicone polymer prevented biofilm and sludge formation after eight weeks of deployment.[50] Although we did not observe biofilm formation on the PVA hydrogel after four weeks of deployment, it is unclear whether the hydrogel deters biofilm and sludge formation. Furthermore, comparison of conventional biliary SEMSs and PSs is important to clarify the significance of the tube-shaped hydrogel as a novel self-expandable biliary stent. Accordingly, longer *in vivo* studies and studies using conventional biliary stents as a control are needed to clarify the significance of the tube-shaped PVA hydrogel.

We here presented the novel concept of using a PVA hydrogel-based self-expandable biliary stent with anisotropic swelling property and endoscopic deliverability. PVA is an inexpensive and biocompatible material eligible for biomedical applications. Moreover, PVA hydrogel can be fabricated with various methods by controlling several properties. For instance, FT cycles improve mechanical strengths and stability.[51,52] In our previous study, we reported the G' (260 $\pm$ 20 kPa) and tear strength values (5.9 $\pm$ 0.5 N mm^{-1}) of the PVA hydrogel used in this study in one FT treatment.[25] As the FT treatment in the present study was also performed once, further improvement in mechanical properties would be expected. Another advantage of the tube-shaped PVA hydrogel is that it can be handled using conventional endoscopic instruments. It would be difficult to replace conventional medical devices, including endoscopes and various other instruments, in function of newly developed devices, given the high cost of such an endeavor. Further *in vivo* experiments and optimization of the PVA hydrogel for application as biliary stents are in progress.

Conclusions

We demonstrated that a tube-shaped PVA hydrogel with anisotropic swelling behavior and endoscopic deliverability has application potential as a self-expandable biliary stent. An *in vivo* experiment using a porcine stent model demonstrated that the tube-shaped PVA hydrogel can expand the biliary tract, without disturbing bile flow. The anisotropic swelling property of PVA hydrogel can be achieved by simple drying, which is accompanied with extension, resulting in a larger I.D. after deployment than that seen in conventional PSs. The WC of the PVA hydrogel is a crucial factor in maintaining endoscopic deliverability. As PVA is inexpensive and

the tube-shaped hydrogel is suitable for use with conventional endoscopic devices, PVA hydrogel is suitable for practical application. Finally, this study demonstrated the novel concept of using a hydrogel stent as a self-expandable biliary stent.

Author contributions

Y. N. conceived and designed the project. Y. N., S. Y., T. T., M. S., K. K., and T. I. performed the experiments and the data analysis. Y. N., S.-i. S. and S. F. discussed the results and wrote the manuscript. All authors reviewed the manuscript.

Funding

This work was partly supported by the Japan Society for the Promotion of Science (JSPS; Grants-in-Aid for Scientific Research, No. 18K07954).

Conflicts of interest

There are no conflicts to declare.

Acknowledgements

The authors would like to thank Kuraray Co., Ltd for kindly providing the PVA samples, Hirosuke Hatayama (Tokyo Metropolitan Industrial Technology Research Institute) for help with the SEM observations, and Editage (www.editage.jp) for English language editing.

References

1 D. H. Ahn and T. Bekaii-Saab, *American Society of Clinical Oncology Educational Book*, 2014, vol. 34, pp. 112–115.
2 N. Razumilava and G. J. Gores, *Lancet*, 2014, **383**, 2168–2179.
3 T. Kamisawa, L. D. Wood, T. Itoi and K. Takaori, *Lancet*, 2016, **388**, 73–85.
4 N. Van der Gaag, J. Kloek, S. de Castro, O. Busch, T. Van Gulik and D. Gouma, *J. Gastrointest. Surg.*, 2009, **13**, 814–820.
5 T. Itoi, F. Itokawa, A. Sofuni, T. Kurihara, K. Ishii, S. Tsuji, N. Ikeuchi, J. Umeda, R. Tanaka, R. Tonozuka and F. Moriyasu, *Endosc. Ultrasound*, 2012, **1**, 36–40.
6 H. Kato, K. Tsutsumi, H. Kawamoto and H. Okada, *World J. Gastrointest. Endosc.*, 2015, **7**, 1032–1038.
7 H. Kawakami, T. Itoi, M. Kuwatani, K. Kawakubo, Y. Kubota and N. Sakamoto, *J. Hepatobiliary Pancreat. Sci.*, 2015, **22**, E12–E21.
8 N. Soehendra and V. Reynders-Frederix, *Endoscopy*, 1980, **12**, 8–11.
9 A. Ballinger, M. McHugh, S. Catnach, E. Alstead and M. Clark, *Gut*, 1994, **35**, 467–470.
10 J.-M. Dumonceau, D. Heresbach, J. Devière, G. Costamagna, U. Beilenhoff and A. Riphaus, *Endoscopy*, 2011, **43**, 617–626.
11 P. R. Pfau, D. K. Pleskow, S. Banerjee, B. A. Barth, Y. M. Bhat, D. J. Desilets, K. T. Gottlieb, J. T. Maple, U. D. Siddiqui and J. L. Tokar, *Gastrointest. Endosc.*, 2013, **77**, 319–327.
12 B. Mangiavillano, N. Pagano, T. H. Baron, M. Arena, G. Iabichino, P. Consolo, E. Opocher and C. Luigiano, *World J. Gastrointest. Endosc.*, 2016, **8**, 143–156.
13 T. Itoi, H. Isayama, A. Sofuni, F. Itokawa, T. Kurihara, T. Tsuchiya, S. Tsuji, K. Ishii, N. Ikeuchi and R. Tanaka, *J. Hepatobiliary Pancreat. Sci.*, 2011, **18**, 664–672.
14 B. J. Hoffman, J. T. Cunningham, W. H. Marsh, J. J. O'Brien and J. Watson, *Gastrointest. Endosc.*, 1994, **40**, 581–583.
15 C. I. Kwon and G. A. Lehman, *Clin. Endosc.*, 2016, **49**, 139–146.
16 K. Huibregtse, J. Cheng, P. Coene, P. Fockens and G. Tytgat, *Endoscopy*, 1989, **21**, 280–282.
17 H. Neuhaus, F. Hagenmüller and M. Classen, *Endoscopy*, 1989, **21**, 225–228.
18 M. J. A. Liberato and J. M. T. Canena, *BMC Gastroenterol.*, 2012, **12**, 103.
19 A. Sangchan, W. Kongkasame, A. Pugkhem, K. Jenwitheesuk and P. Mairiang, *Gastrointest. Endosc.*, 2012, **76**, 93–99.
20 T. Itoi, A. Sofuni, F. Itokawa, R. Tonozuka and K. Ishii, *Dig. Endosc.*, 2013, **25**, 63–70.
21 N. Vakil, A. I. Morris, N. Marcon, A. Segalin, A. Peracchia, N. Bethge, G. Zuccaro, J. J. Bosco and W. F. Jones, *Am. J. Gastroenterol.*, 2001, **96**, 1791–1796.
22 H. Isayama, Y. Komatsu, T. Tsujino, N. Sasahira, K. Hirano, N. Toda, Y. Nakai, N. Yamamoto, M. Tada and H. Yoshida, *Gut*, 2004, **53**, 729–734.
23 H. Isayama, Y. Nakai, H. Kogure, N. Yamamoto and K. Koike, *Dig. Endosc.*, 2013, **25**, 71–74.
24 A. Tringali, C. Hassan, M. Rota, M. Rossi, M. Mutignani and L. Aabakken, *Endoscopy*, 2018, **50**, 631–641.
25 Y. Nagakawa, S. Fujita, S. Yunoki, T. Tsuchiya, S. i. Suye and T. Itoi, *J. Appl. Polym. Sci.*, 2020, **137**, 48851.
26 C. M. Hassan and N. A. Peppas, *Macromolecules*, 2000, **33**, 2472–2479.
27 E. Otsuka and A. Suzuki, *J. Appl. Polym. Sci.*, 2009, **114**, 10–16.
28 T. Fukumori and T. Nakaoki, *J. Appl. Polym. Sci.*, 2014, **131**, 40578.
29 S. Muppalaneni and H. Omidian, *J. Dev. Drugs*, 2013, **2**(3), 1000112.
30 W. Wan, A. D. Bannerman, L. Yang and H. Mak, in *Polymeric Cryogels*, Springer, 2014, pp. 283–321.
31 M. Kokabi, M. Sirousazar and Z. M. Hassan, *Eur. Polym. J.*, 2007, **43**, 773–781.
32 S. Yunoki, M. Kohta, Y. Ohyabu, M. Sekiguchi, T. Kubo and T. Iwasaki, *J. Appl. Polym. Sci.*, 2014, **131**, 40456.
33 S.-H. Hyon, W.-I. Cha, Y. Ikada, M. Kita, Y. Ogura and Y. Honda, *J. Biomater. Sci., Polym. Ed.*, 1994, **5**, 397–406.
34 M. I. Baker, S. P. Walsh, Z. Schwartz and B. D. Boyan, *J. Biomed. Mater. Res., Part B*, 2012, **100**, 1451–1457.
35 J. Negishi, K. Nam, T. Kimura, Y. Hashimoto, S. Funamoto, T. Higami, T. Fujisato and A. Kishida, *J. Biomed. Mater. Res., Part B*, 2014, **102**, 1426–1433.
36 D. Moreau, A. Villain, M. Bachy, H. Proudhon, D. N. Ku, D. Hannouche, H. Petite and L. Corté, *J. Mater. Sci.: Mater. Med.*, 2017, **28**, 114.

37 Y. Hou, W. Xie, K. Achazi, J. L. Cuellar-Camacho, M. F. Melzig, W. Chen and R. Haag, *Acta Biomater.*, 2018, **77**, 28–37.
38 C. Curley, J. C. Hayes, N. J. Rowan and J. E. Kennedy, *J. Mech. Behav. Biomed. Mater.*, 2014, **40**, 13–22.
39 T. Miyazaki, A. Hoshiko, M. Akasaka, T. Shintani and S. Sakurai, *Macromolecules*, 2006, **39**, 2921–2929.
40 S. Yunoki, H. Sugiura, T. Ikoma, E. Kondo, K. Yasuda and J. Tanaka, *Biomed. Mater.*, 2011, **6**, 015012.
41 T. Yano, Y. Higaki, D. Tao, D. Murakami, M. Kobayashi, N. Ohta, J.-i. Koike, M. Horigome, H. Masunaga and H. Ogawa, *Polymer*, 2012, **53**, 4702–4708.
42 M. Oyen, *Int. Mater. Rev.*, 2014, **59**, 44–59.
43 H. Kamata, Y. Akagi, Y. Kayasuga-Kariya, U.-i. Chung and T. Sakai, *Science*, 2014, **343**, 873–875.
44 D. R. Schmidt, H. Waldeck and W. J. Kao, in *Biological interactions on materials surfaces*, Springer, 2009, pp. 1–18.
45 P. H. Deprez, T. G. Moreels, T. Aouattah, H. Piessevaux and E. Pérez-Cuadrado-Robles, *Endoscopy*, 2020, **52**, 474–482.
46 B. Chu and B. S. Hsiao, *Chem. Rev.*, 2001, **101**, 1727–1761.
47 G. Sridharan and A. A. Shankar, *J. Oral Maxillofac. Pathol.*, 2012, **16**, 251.
48 H.-C. Flemming and J. Wingender, *Nat. Rev. Microbiol.*, 2010, **8**, 623–633.
49 J. Azeredo, N. F. Azevedo, R. Briandet, N. Cerca, T. Coenye, A. R. Costa, M. Desvaux, G. Di Bonaventura, M. Hébraud and Z. Jaglic, *Crit. Rev. Microbiol.*, 2017, **43**, 313–351.
50 T. H. Lee, B. S. Jang, M. K. Jung, C. G. Pack, J. H. Choi and D. H. Park, *Sci. Rep.*, 2016, **6**, 35446.
51 H. Adelnia, R. Ensandoost, S. S. Moonshi, J. N. Gavgani, E. I. Vasafi and H. T. Ta, *Eur. Polym. J.*, 2022, **164**, 110974.
52 Y. Nagakawa, M. Kato, S.-i. Suye and S. Fujita, *RSC Adv.*, 2020, **10**, 38045–38054.